Study of the Perturbation Series for the Ground-State Energy of a Many-Fermion System*

GEORGE A. BAKER, JR., J. L. GAMMEL, AND B. J. HILL
Los Alamos Scientific Laboratory, University of California, Los Alamos, New Mexico
(Received 26 June 1963)

In order to investigate the validity of the Brueckner and the simple sum of the ladder diagrams approximations to the energy of an infinite system of fermions, we have calculated as a function of density all the terms in the perturbation expansion through the fourth order in the strength of the potential. We have done this for a repulsive, square-well, two-body potential spin-$\frac{1}{2}$ fermions. We are able to construct rigorous upper and lower bounds from the coefficients for the value of the ladder approximation and find that the standard solution procedures give reasonably accurate results (within a few percent). We find that the error in the solution as obtained in practice to the equations of the Brueckner approximation is large compared to the size of its departure from the ladder approximation. We further find for low-to-moderate densities and for low-to-moderate potential strengths that the Brueckner approximation both as a sum of a certain class of diagrams and as computed in practice lies above the ladder approximation while the complete perturbation theory lies below it. This result arises from the neglect of the ring diagrams by the Brueckner approximation.

I. INTRODUCTION

THE Brueckner theory contains two classes of approximations. The first class of approximations are numerical in character, introduced to make calculations feasible. The Pauli exclusion principle is not treated exactly; neither is the dependence of the K matrices on the total momentum treated exactly; approximations are introduced to make a partial-wave expansion of the K-matrix equations possible. Off-energy shell propagation is not treated exactly either; an approximation is introduced to simplify this formidable aspect of the Brueckner theory. The other class of approximations is the neglect of diagrams in every order (beyond the second) of many-body perturbation theory.

Actual calculations of Brueckner theory reveal unexpected results: For example, Brueckner and Gammel found that the self-consistency problem has no solution for liquid He^3 for densities larger than a certain critical density.[1] Is this result a consequence of the theory or the numerical approximations? Our results suggest that it is a consequence of the treatment of off-energy shell propagation.

Our purpose is to investigate these approximations for a simple, realistic problem, namely, a system of identical spin-$\frac{1}{2}$ particles (liquid He^3, for example) interacting via a square-well potential, an extreme limit of which is a repulsive hard core.

A method which has influenced our thinking is the Padé approximant method.[2] This method offers a way of summing perturbation series which is different from Brueckner's K-matrix method. The Padé method does not require a partial-wave expansion or approximate treatment of the off-energy shell effects, and all diagrams in any given order can be included. Thus, we hope to learn something about the effects of approximations used in the Brueckner calculations, and to answer questions such as that raised by the Brueckner-Gammel calculations in liquid He^3.

Deeper questions of the convergence of the perturbation series have been dealt with in a paper by one of the present authors[3] (G.B.). We show in this paper that the sum of the ladder diagrams is bounded from above by the $[n, n+1]$ Padé approximants and from below by the $[n,n]$ Padé approximants.

An outline of our program is: First, a calculation of all terms in perturbation theory through fourth order, without approximation. These results are of interest independently of the rest of our work; they show that the most important diagrams, other than the ladder diagrams, at low density are not the self-energy diagrams but the ring diagrams,[4] the same diagrams which are most important at high density.[5]

Second, a calculation of the sum of the ladder diagrams and the sum of the Brueckner diagrams for various potential depths, using all the approximations ordinarily used in calculating Brueckner theory. Since we calculate the results for many potential depths, the series expansions through any order may be found by standard numerical techniques. By other techniques we separate the contributions of various diagrams in each order. Thus, we may compare the calculations of the first part of our program and the calculations of the

* Work performed under the auspices of the U. S. Atomic Energy Commission.

[1] K. A. Brueckner and J. L. Gammel, Phys. Rev. **109**, 1040 (1958), Sec. D.

[2] G. A. Baker, Jr. and J. L. Gammel, J. Math. Anal. Appl. **2**, 21 (1961). G. A. Baker, Jr., J. L. Gammel, and J. G. Wills, J. Math. Anal. Appl. **2**, 405 (1961). H. S. Wall, *Continued Fractions* (D. Van Nostrand, Inc., Princeton, New Jersey), Chap. XX.

[3] G. A. Baker, Jr., Phys. Rev. **131**, 1869 (1963).

[4] It can be shown that this result is independent of the shape of the potential. In private conversation, K. A. Brueckner has suggested that this result may not hold near equilibrium densities for realistic potentials with long-range attractions and short-range repulsions. We do not, however, have any direct evidence on this point although Bethe's estimate [H. A. Bethe, Phys. Rev. **103**, 1353 (1956)] suggests it may be so for nuclear matter. See also the discussion of N. M. Hugenholtz (Ref. 5, p. 542).

[5] N. M. Hugenholtz, Physica **23**, 533 (1957), Table on p. 542.

second part of our program to find how the approximations ordinarily used in calculating Brueckner theory affect the contribution of any particular diagram.

Thirdly, using the rigorous bounds established for the sum of the ladder diagrams, and the exact calculations done in the first part of our program, we are able to assess the numerical consequences of the approximations ordinarily used in calculating Brueckner theory in so far as they affect the sum of the ladder diagrams. We also attempt to assess these numerical consequences in so far as they affect the sum of the Brueckner diagrams, although our results are not completely rigorous because the Padé method does not give bounds in this case. Finally, we assess the numerical importance of diagrams omitted by Brueckner by including contributions of all diagrams in forming the Padé approximants but our results are subject to the criticism just mentioned; namely, that the Padé approximants do not give bounds for the complete series, although it likely gives a very good estimate of the value.

Our conclusions are as follows. The numerical approximations made in evaluating the Brueckner theory are of no particular consequence, except for the treatment of off-energy shell propagation. The effects of this approximation are such that the opposite sign is obtained for the correction to the fourth order (the first order in which this approximation appears) ladder diagram for low ($k_{FC}<1$) density. This error severely affects the numerical content of the Brueckner theory. As mentioned before, we believe this error to be the origin of the difficulty encountered by Brueckner and Gammel.

We find that the sum of the complete series lies on the opposite side of the sum of the ladder diagrams from the Brueckner theory for low-to-moderate densities and low-to-moderate potential strengths.

II. THE LOW ORDER TERMS IN THE MANY-FERMION PERTURBATION SERIES

We shall now describe the calculation of all the terms through fourth order in the interaction potential in the Goldstone[6] expansion of the ground-state energy per particle of a system of many spin-$\frac{1}{2}$ fermions. We first write out the integral for each Hugenholtz[7] diagram and then perform these integrals by a Monte Carlo procedure on the IBM 7030. The potential taken is that for a square well of width c and depth V. The momentum transform is proportional to

$$v(q)=(4\pi/q^3)(\sin qk_{FC}-qk_{FC}\cos qk_{FC}), \quad (2.1)$$

where q, measured in units of the Fermi momentum, is the momentum transfer in the interaction. We will obtain terms in the expansion

$$\Delta EMc^2/(N\hbar^2)=A_1(VMc^2/\hbar^2)+A_2(VMc^2/\hbar^2)^2 +A_3(VMc^2/\hbar^2)^3+\cdots. \quad (2.2)$$

The contribution A_1 comes solely from Fig. 1(a). It is

$$3/(2^5\pi^4)\int_{|\mathbf{m}|\leq 1,|\mathbf{n}|\leq 1} d\mathbf{m}d\mathbf{n}[v(0)-\tfrac{1}{2}v(|\mathbf{m}-\mathbf{n}|)], \quad (2.3)$$

where $\mathbf{m}$ and $\mathbf{n}$ are the momenta scaled by k_F, the momentum at the top of the Fermi sea. This integral may be done analytically in terms of the sine integral $\mathrm{Si}(x)$: The result is

$$\frac{(k_{FC})^3}{9\pi}\left\{2-\frac{72}{x^6}[x^3\,\mathrm{Si}(x)-4-3x^2+(4+x^2)\cos x +4x\sin x]\right\}, \quad (2.4)$$

where x is $2k_{FC}$.

The contribution A_2 comes solely from Fig. 1(b). (We denote holes by lines running left to right and filled-state lines vice versa.) It is

$$-3/[2^8\pi^7(k_{FC})^2] \times\int d\mathbf{m}d\mathbf{n}d\mathbf{q}\frac{v(q)[v(q)-\frac{1}{2}v(|\mathbf{n}-\mathbf{m}-\mathbf{q}|)]}{q^2+\mathbf{q}\cdot(\mathbf{m}-\mathbf{n})}, \quad (2.5)$$

where the integration is carried over all values allowed by the Pauli exclusion principle; that is, all hole-line momenta are in the Fermi sea and all filled state-line momenta are outside the Fermi sea. We select the independent momenta in the Fermi sea according to the prescription that, say, $m^3=r_1$, where r_1 is a random number which is distributed uniformly on the interval

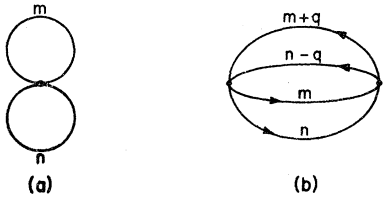

FIG. 1. First, and second-order perturbation theory diagrams.

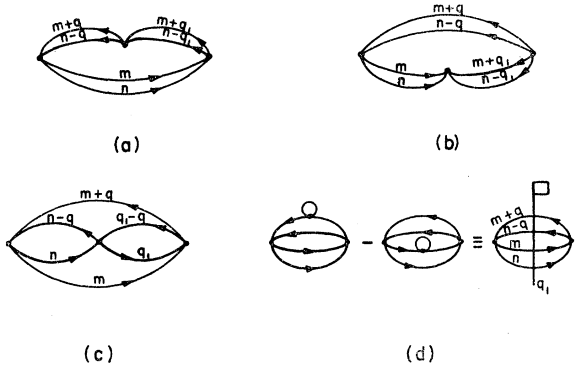

FIG. 2. Third-order perturbation theory diagrams.

[6] J. Goldstone, Proc. Roy. Soc. (London) **A239**, 267 (1957).
[7] N. M. Hugenholtz, Physica **23**, 481 (1957).

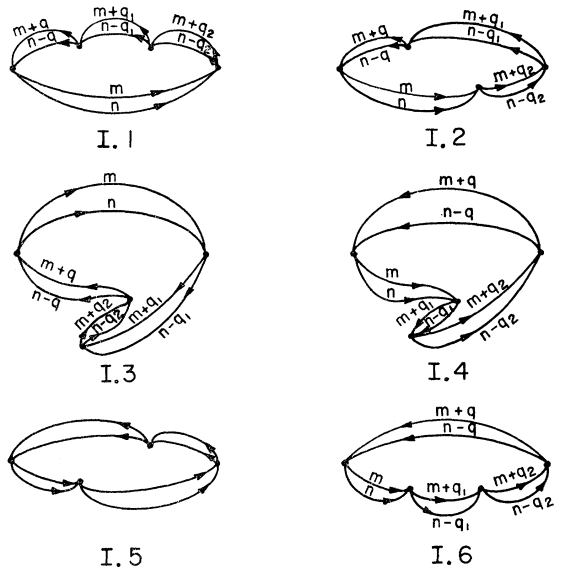

FIG. 3. Class I, Fourth-order perturbation theory diagrams.

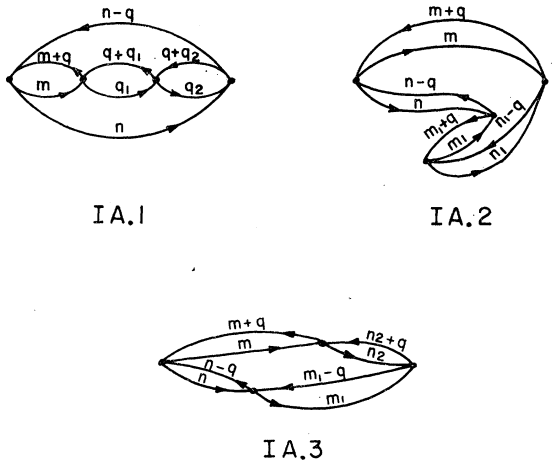

FIG. 4. Class IA, Fourth-order perturbation theory diagrams.

(0,1). For momenta which can be infinite, we select a filled-state momentum, say $|\mathbf{m}+\mathbf{q}|=r_2^{-E}$, where r_2 is again a random number which is uniformly distributed on the interval (0,1). The parameter E is selected so that the integrand goes to a constant as r_2 goes to zero. For the second-order calculation, for example, $E=\frac{1}{3}$. In other diagrams we will get terms like $v(\mathbf{q}-\mathbf{q}_1)$, where both q and q_1 go to infinity. The proper power counting procedure here, as we have previously pointed out,[3] is to treat this term at infinity like $1/(qq_1)$.

The contribution to A_3 comes from the four separate diagrams shown in Fig. 2. For a further explanation for the "flag" notation [Fig. 2(d)], see Ref. 3. The various contributions are:

Fig. 2(a):

$$\mathrm{B3}=3/[2^{11}\pi^{10}(k_FC)^4]\int\frac{d\mathbf{m}d\mathbf{n}d\mathbf{q}d\mathbf{q}_1v(q)v(|\mathbf{q}-\mathbf{q}_1|)[v(\mathbf{q}_1)-\frac{1}{2}v(|\mathbf{m}-\mathbf{n}+\mathbf{q}_1|)]}{[q^2+\mathbf{q}\cdot(\mathbf{m}-\mathbf{n})][q_1^2+\mathbf{q}_1\cdot(\mathbf{m}-\mathbf{n})]},\tag{2.6}$$

Fig. 2(b):

$$\mathrm{H3}=3/[2^{11}\pi^{10}(k_FC)^4]\int\frac{d\mathbf{m}d\mathbf{n}d\mathbf{q}d\mathbf{q}_1v(q)v(q_1)[v(|\mathbf{q}-\mathbf{q}_1|)-\frac{1}{2}v(|\mathbf{q}+\mathbf{q}_1+\mathbf{m}-\mathbf{n}|)]}{[q^2+\mathbf{q}\cdot(\mathbf{m}-\mathbf{n})][q^2-q_1^2+(\mathbf{q}-\mathbf{q}_1)\cdot(\mathbf{m}-\mathbf{n})]},\tag{2.7}$$

Fig. 2(c):

$$\mathrm{R3}=3/[2^9\pi^{10}(k_FC)^4]\int\frac{d\mathbf{m}d\mathbf{n}d\mathbf{q}d\mathbf{q}_1[v(q)-\frac{1}{2}v(|\mathbf{m}+\mathbf{q}-\mathbf{q}_1|)]}{[q^2+\mathbf{q}\cdot(\mathbf{m}-\mathbf{n})]}$$
$$\times\frac{[v(q)-\frac{1}{2}v(|\mathbf{n}-\mathbf{q}_1|)][v(q)-\frac{1}{2}v(|\mathbf{n}-\mathbf{m}-\mathbf{q}|)]-\frac{3}{8}v(|\mathbf{n}-\mathbf{m}-\mathbf{q}|)v(|\mathbf{m}+\mathbf{q}-\mathbf{q}_1|)v(|\mathbf{n}-\mathbf{q}_1|)}{[q^2+\mathbf{q}\cdot(\mathbf{m}-\mathbf{q}_1)]},\tag{2.8}$$

Fig. 2(d):

$$\mathrm{F3}=-3/[(2\pi)^{10}(k_FC)^4]\int\frac{d\mathbf{m}d\mathbf{n}d\mathbf{q}d\mathbf{q}_1v(q)[v(q)-\frac{1}{2}v(|\mathbf{n}-\mathbf{m}-\mathbf{q}|)]}{[q^2+\mathbf{q}\cdot(\mathbf{m}-\mathbf{n})]^2}[v(|\mathbf{q}+\mathbf{m}+\mathbf{q}_1|)-v(|\mathbf{m}+\mathbf{q}_1|)].\tag{2.9}$$

There are 46 diagrams which contribute to fourth order. Of these 46 there are only 28 distinct, nonzero ones. To facilitate the cataloging of them, we will break them down into classes. Those diagrams of class I are shown in Fig. 3. The contributions are all of the form

$$-3/[2^{14}\pi^{13}(k_FC)^3]\int\frac{d\mathbf{m}d\mathbf{n}d\mathbf{q}d\mathbf{q}_1d\mathbf{q}_2v(q)v(x_2)v(x_3)[v(x_4)-\frac{1}{2}v(x_5)]}{[q^2+\mathbf{q}\cdot(\mathbf{m}-\mathbf{n})]D_2D_3}.\tag{2.10}$$

The values of x_i and D_i are listed in Table I. It is to be noted that I.5 is identical to I.2. For simplicity we may

TABLE I. Arguments of the potentials and denominators.

Diagram	x_2	x_3	x_4	x_5	D_2	D_3
I.1	$\lvert\mathbf{q}-\mathbf{q}_1\rvert$	$\lvert\mathbf{q}_1-\mathbf{q}_2\rvert$	q_2	$\lvert\mathbf{n}-\mathbf{m}-\mathbf{q}_2\rvert$	$q_1^2+\mathbf{q}_1\cdot(\mathbf{m}-\mathbf{n})$	$q_2^2+\mathbf{q}_2\cdot(\mathbf{m}-\mathbf{n})$
I.2	$\lvert\mathbf{q}-\mathbf{q}_1\rvert$	$\lvert\mathbf{q}_1-\mathbf{q}_2\rvert$	q_2	$\lvert\mathbf{n}-\mathbf{m}-\mathbf{q}_2\rvert$	$q_1^2+\mathbf{q}_1\cdot(\mathbf{m}-\mathbf{n})$	$q_1^2-q_2^2+(\mathbf{q}_1-\mathbf{q}_2)\cdot(\mathbf{m}-\mathbf{n})$
I.3+4	$\lvert\mathbf{q}_2-\mathbf{q}_1\rvert$	$\lvert\mathbf{q}-\mathbf{q}_2\rvert$	q_1	$\lvert\mathbf{n}-\mathbf{m}-\mathbf{q}_1\rvert$	$q_1^2+\mathbf{q}_1\cdot(\mathbf{m}-\mathbf{n})$	$q^2-q_2^2+(\mathbf{q}-\mathbf{q}_2)\cdot(\mathbf{m}-\mathbf{n})$
I.6	$\lvert\mathbf{q}-\mathbf{q}_2\rvert$	$\lvert\mathbf{q}_2-\mathbf{q}_1\rvert$	q_1	$\lvert\mathbf{n}-\mathbf{m}-\mathbf{q}_1\rvert$	$q^2-q_1^2+(\mathbf{q}-\mathbf{q}_1)\cdot(\mathbf{m}-\mathbf{n})$	$q^2-q_2^2+(\mathbf{q}-\mathbf{q}_2)\cdot(\mathbf{m}-\mathbf{n})$
IA.1	$\lvert\mathbf{n}-\mathbf{m}-\mathbf{q}\rvert$	$\lvert\mathbf{q}_1-\mathbf{m}\rvert$	$\lvert\mathbf{q}_1-\mathbf{q}_2\rvert$	$\lvert\mathbf{n}-\mathbf{q}-\mathbf{q}_2\rvert$	$q^2+\mathbf{q}\cdot(\mathbf{q}_1-\mathbf{n})$	$q^2+\mathbf{q}\cdot(\mathbf{q}_2-\mathbf{n})$
IA.2	$\lvert\mathbf{n}-\mathbf{m}-\mathbf{q}\rvert$	$\lvert\mathbf{n}_1-\mathbf{m}_1-\mathbf{q}\rvert$	$\lvert\mathbf{n}-\mathbf{m}_1-\mathbf{q}\rvert$	$\lvert\mathbf{n}_1-\mathbf{m}-\mathbf{q}\rvert$	$2q^2+\mathbf{q}\cdot(\mathbf{m}+\mathbf{m}_1-\mathbf{n}-\mathbf{n}_1)$	$q^2+\mathbf{q}\cdot(\mathbf{m}-\mathbf{n})$
IA.3	$\lvert\mathbf{n}-\mathbf{m}-\mathbf{q}\rvert$	$\lvert\mathbf{n}-\mathbf{m}_1\rvert$	$\lvert\mathbf{n}_2-\mathbf{m}\rvert$	$\lvert\mathbf{n}_2-\mathbf{m}_1+\mathbf{q}\rvert$	$q^2+\mathbf{q}\cdot(\mathbf{m}-\mathbf{m}_1)$	$q^2+\mathbf{q}\cdot(\mathbf{n}_2-\mathbf{m}_1)$

combine I.3 and I.4. The diagrams in class IA are illustrated in Fig. 4 and all have contributions of the form

$$-3/[2^{11}\pi^{13}(k_FC)^3]\int \frac{d\tau[v(q)-\frac{1}{2}v(x_2)][v(q)-\frac{1}{2}v(x_3)][v(q)-\frac{1}{2}v(x_4)][v(q)-\frac{1}{2}v(x_5)]+\frac{3}{16}v(x_2)v(x_3)v(x_4)v(x_5)}{[q^2+\mathbf{q}\cdot(\mathbf{m}-\mathbf{n})]D_2D_3}, \quad (2.11)$$

where $d\tau$ is the volume element and the x_i and D_i are given in Table I. The diagrams in class II are illustrated in Fig. 5 and all have contributions of the form

$$-3/[2^{12}\pi^{13}(k_FC)^6]\int \frac{d\tau v(x_1)[v(x_2)-\frac{1}{2}v(x_3)][v(x_4)-\frac{1}{2}v(x_5)][v(x_4)-\frac{1}{2}v(x_6)]-\frac{3}{8}v(x_1)\,v(x_3)v(x_5)v(x_6)}{[q^2+\mathbf{q}\cdot(\mathbf{m}-\mathbf{n})]D_2D_3}, \quad (2.12)$$

except, where indicated in the figure by a minus sign, there is the opposite sign. The x_i and D_i are given in Table II. The contribution of II.2 is identical with that of II.1, II.3 with II.4, II.7 with II.12, and II.8 with II.11. The diagrams in class II A are illustrated in Fig. 6 and all have contributions of the form

$$-3/[2^{11}\pi^{13}(k_FC)^6]\int \frac{d\tau T}{[q^2+\mathbf{q}\cdot(\mathbf{m}-\mathbf{n})]D_2D_3}, \quad (2.13)$$

where

$$T=v(x_1)^2[v(x_3)^2+v(x_4)v(x_6)]+v(x_2)v(x_5)v(x_3)^2-\tfrac{1}{2}\{v(x_3)[v(x_1)^2+v(x_2)v(x_5)][v(x_6)+v(x_4)]$$
$$+v(x_1)[v(x_3)^2+v(x_4)v(x_6)][v(x_5)+v(x_2)]\}+\tfrac{1}{4}\{v(x_1)v(x_3)[v(x_2)+v(x_5)][v(x_4)+v(x_6)]+T_1\}, \quad (2.14)$$

except for the noted sign changes. The x_i and D_i are given in Table II. The contribution of IIA.2 is identical with that of IIA.4. For T_1 we have

$$\begin{aligned} T_1&=v(x_2)v(x_4)v(x_5)v(x_6) \quad \text{for} \quad \text{IIA.1–4} \\ T_1&=v(x_4)v(x_6)v(x_1)^2 \quad \text{for} \quad \text{IIA.5–6.} \end{aligned} \quad (2.15)$$

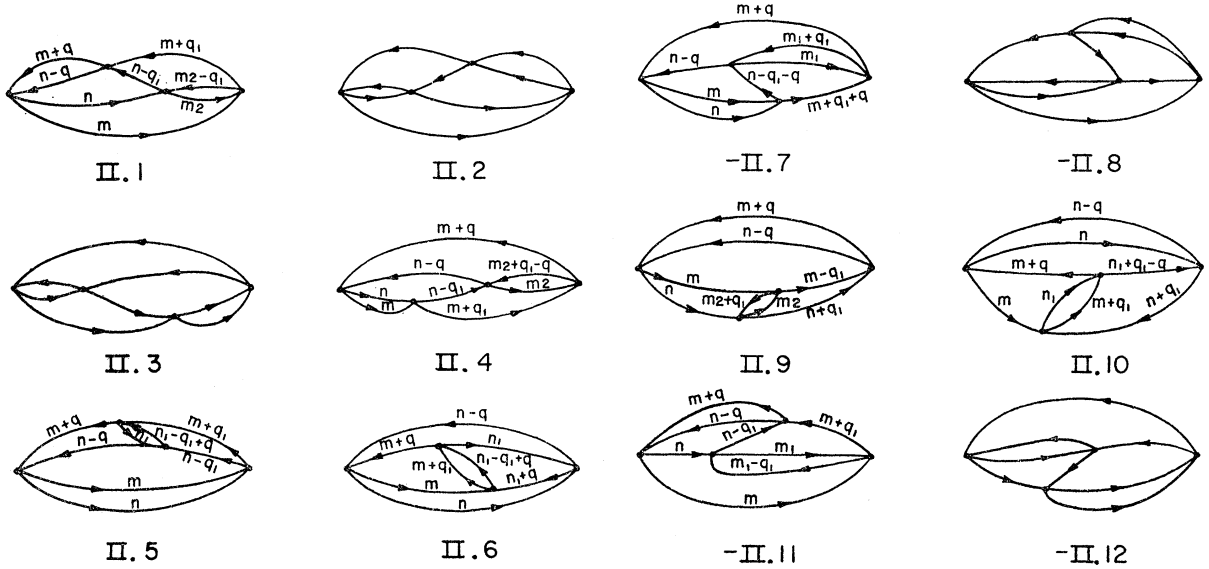

FIG. 5. Class II, Fourth-order perturbation theory diagrams.

TABLE II. Arguments of the potentials and denominators.

Diagram	x_1	x_2	x_3	x_4
II.1	q	$\lvert\mathbf{q}-\mathbf{q}_1\rvert$	$\lvert\mathbf{n}-\mathbf{m}-\mathbf{q}-\mathbf{q}_1\rvert$	q_1
II.4	q	q_1	$\lvert\mathbf{n}-\mathbf{m}-\mathbf{q}_1\rvert$	$\lvert\mathbf{q}-\mathbf{q}_1\rvert$
II.5	q	q_1	$\lvert\mathbf{n}-\mathbf{m}-\mathbf{q}_1\rvert$	$\lvert\mathbf{q}-\mathbf{q}_1\rvert$
II.6	q_1	$\lvert\mathbf{q}_1-\mathbf{q}\rvert$	$\lvert\mathbf{n}_1-\mathbf{m}-\mathbf{q}_1\rvert$	q
II.7	q	$\lvert\mathbf{q}+\mathbf{q}_1\rvert$	$\lvert\mathbf{n}-\mathbf{m}-\mathbf{q}_1-\mathbf{q}\rvert$	q_1
II.9	q	$\lvert\mathbf{q}-\mathbf{q}_1\rvert$	$\lvert\mathbf{n}-\mathbf{m}+\mathbf{q}_1-\mathbf{q}\rvert$	q_1
II.10	q_1	$\lvert\mathbf{q}-\mathbf{q}_1\rvert$	$\lvert\mathbf{n}_1-\mathbf{m}-\mathbf{q}\rvert$	q
II.11	q	$\lvert\mathbf{q}_1-\mathbf{q}\rvert$	$\lvert\mathbf{n}-\mathbf{m}-\mathbf{q}-\mathbf{q}_1\rvert$	q_1
IIA.1	q	$\lvert\mathbf{n}-\mathbf{m}-\mathbf{q}\rvert$	q_1	$\lvert\mathbf{n}-\mathbf{m}_1-\mathbf{q}-\mathbf{q}_1\rvert$
IIA.2	q	$\lvert\mathbf{n}-\mathbf{m}-\mathbf{q}\rvert$	q_1	$\lvert\mathbf{n}-\mathbf{m}_1-\mathbf{q}-\mathbf{q}_1\rvert$
IIA.3	q	$\lvert\mathbf{n}-\mathbf{m}-\mathbf{q}\rvert$	q_1	$\lvert\mathbf{n}-\mathbf{m}_1\rvert$
IIA.5	$\lvert\mathbf{q}_1-\mathbf{q}\rvert$	$\lvert\mathbf{m}_2-\mathbf{m}-\mathbf{q}\rvert$	$\lvert\mathbf{n}-\mathbf{m}-\mathbf{q}\rvert$	q
IIA.6	$\lvert\mathbf{q}_1-\mathbf{q}\rvert$	$\lvert\mathbf{n}-\mathbf{n}_2-\mathbf{q}+\mathbf{q}_1\rvert$	$\lvert\mathbf{n}-\mathbf{m}-\mathbf{q}\rvert$	q

Diagram	x_5	x_6	D_2	D_3
II.1	$\lvert\mathbf{n}-\mathbf{m}_2\rvert$	$\lvert\mathbf{m}_2-\mathbf{m}-\mathbf{q}_1\rvert$	$q_1^2+\mathbf{q}_1\cdot(\mathbf{m}-\mathbf{n})$	$q_1^2+\mathbf{q}_1\cdot(\mathbf{m}-\mathbf{m}_2)$
II.4	$\lvert\mathbf{n}-\mathbf{m}_2-\mathbf{q}_1\rvert$	$\lvert\mathbf{m}_2-\mathbf{m}-\mathbf{q}\rvert$	$q^2-q_1^2+(\mathbf{q}-\mathbf{q}_1)\cdot(\mathbf{m}-\mathbf{n})$	$q^2+\mathbf{q}\cdot(\mathbf{m}-\mathbf{m}_2-\mathbf{q}_1)+\mathbf{q}_1\cdot(\mathbf{m}_2-\mathbf{m})$
II.5	$\lvert\mathbf{n}_1-\mathbf{m}-\mathbf{q}_1\rvert$	$\lvert\mathbf{n}-\mathbf{n}_1-\mathbf{q}\rvert$	$q_1^2+\mathbf{q}_1\cdot(\mathbf{m}-\mathbf{n})$	$q_1^2+\mathbf{q}_1\cdot(\mathbf{m}-\mathbf{n}_1-\mathbf{q})+q^2+\mathbf{q}\cdot(\mathbf{n}_1-\mathbf{n})$
II.6	$\lvert\mathbf{n}-\mathbf{m}-\mathbf{q}\rvert$	$\lvert\mathbf{n}_1-\mathbf{n}+\mathbf{q}\rvert$	$q^2+\mathbf{q}\cdot(\mathbf{n}_1-\mathbf{n})$	$q_1^2+\mathbf{q}_1\cdot(\mathbf{m}-\mathbf{n}_1-\mathbf{q})+q^2+\mathbf{q}\cdot(\mathbf{n}_1-\mathbf{n})$
II.7	$\lvert\mathbf{m}_1-\mathbf{m}-\mathbf{q}\rvert$	$\lvert\mathbf{n}-\mathbf{m}_1-\mathbf{q}-\mathbf{q}_1\rvert$	$q^2+\mathbf{q}\cdot(\mathbf{m}-\mathbf{n}+\mathbf{q}_1)+q_1^2+\mathbf{q}_1\cdot(\mathbf{m}_1-\mathbf{n})$	$\mathbf{q}_1\cdot(\mathbf{m}_1-\mathbf{m}-\mathbf{q})$
II.9	$\lvert\mathbf{n}-\mathbf{m}_2\rvert$	$\lvert\mathbf{m}_2-\mathbf{m}+\mathbf{q}_1\rvert$	$q^2+\mathbf{q}\cdot(\mathbf{m}-\mathbf{n})+\mathbf{q}_1\cdot(\mathbf{m}_2-\mathbf{n})$	$q^2-q_1^2+(\mathbf{q}+\mathbf{q}_1)\cdot(\mathbf{m}-\mathbf{n})$
II.10	$\lvert\mathbf{n}-\mathbf{m}-\mathbf{q}\rvert$	$\lvert\mathbf{n}_1-\mathbf{n}+\mathbf{q}_1\rvert$	$q^2+\mathbf{q}\cdot(\mathbf{m}-\mathbf{n})-\mathbf{q}_1\cdot(\mathbf{m}-\mathbf{n}_1)$	$\mathbf{q}\cdot(\mathbf{q}_1-\mathbf{n}+\mathbf{n}_1)$
II.11	$\lvert\mathbf{n}-\mathbf{m}_1\rvert$	$\lvert\mathbf{m}-\mathbf{m}_1+\mathbf{q}_1\rvert$	$q_1^2+\mathbf{q}\cdot(\mathbf{m}-\mathbf{m}_1)$	$q^2+\mathbf{q}\cdot(\mathbf{m}-\mathbf{n})-\mathbf{q}_1\cdot(\mathbf{m}_1-\mathbf{n})$
IIA.1	$\lvert\mathbf{n}-\mathbf{m}-\mathbf{q}-\mathbf{q}_1\rvert$	$\lvert\mathbf{n}-\mathbf{m}_1-\mathbf{q}_1\rvert$	$q_1^2+\mathbf{q}_1\cdot(\mathbf{m}_1-\mathbf{n})$	$q^2+\mathbf{q}\cdot(\mathbf{q}_1+\mathbf{m}-\mathbf{n})+q_1^2+\mathbf{q}_1\cdot(\mathbf{m}_1-\mathbf{n})$
IIA.2	$\lvert\mathbf{n}-\mathbf{m}-\mathbf{q}-\mathbf{q}_1\rvert$	$\lvert\mathbf{n}-\mathbf{m}_1-\mathbf{q}_1\rvert$	$q^2+\mathbf{q}\cdot(\mathbf{m}-\mathbf{n}+\mathbf{q}_1)$	$q^2+\mathbf{q}\cdot(\mathbf{q}_1+\mathbf{m}-\mathbf{n})+q_1^2+\mathbf{q}_1\cdot(\mathbf{m}_1-\mathbf{n})$
IIA.3	$\lvert\mathbf{n}-\mathbf{m}-\mathbf{q}+\mathbf{q}_1\rvert$	$\lvert\mathbf{n}-\mathbf{m}_1-\mathbf{q}\rvert$	$q^2+\mathbf{q}\cdot(\mathbf{m}-\mathbf{n})+\mathbf{q}_1\cdot(\mathbf{m}_1-\mathbf{n})$	$\mathbf{q}_1\cdot(\mathbf{m}_1-\mathbf{n}+\mathbf{q})$
IIA.5	$\lvert\mathbf{n}-\mathbf{m}_2\rvert$	q_1	$q^2+\mathbf{q}\cdot(\mathbf{m}-\mathbf{n}-\mathbf{q}_1)+\mathbf{q}_1\cdot(\mathbf{n}-\mathbf{m})$	$q^2+\mathbf{q}\cdot(\mathbf{m}-\mathbf{m}_2-\mathbf{q}_1)+\mathbf{q}_1\cdot(\mathbf{m}_2-\mathbf{m})$
IIA.6	$\lvert\mathbf{n}_2-\mathbf{m}-\mathbf{q}_1\rvert$	q_1	$q^2+\mathbf{q}\cdot(\mathbf{m}-\mathbf{n}-\mathbf{q}_1)+\mathbf{q}_1\cdot(\mathbf{n}-\mathbf{m})$	$(\mathbf{q}-\mathbf{q}_1)^2+(\mathbf{q}-\mathbf{q}_1)\cdot(\mathbf{n}_2-\mathbf{n})$

The diagrams of class III are illustrated in Fig. 7. Diagrams 3, 4, 5, 6, 11, and 12 vanish because they have (by momentum conservation) a hole and a filled state line with the same momentum. We have combined 7 and 8, and 9 and 10 for convenience. All the contributions have the form

$$-3/[2^{12}\pi^{13}(k_{FC})^6]\int\frac{d\tau v(q)[v(q)-\frac{1}{2}v(|\mathbf{n}-\mathbf{m}-\mathbf{q}|)]v(x_2)[v(x_2)-\frac{1}{2}v(x_3)]}{[q^2+\mathbf{q}\cdot(\mathbf{m}-\mathbf{n})]^2D_3}, \tag{2.16}$$

where the x_i and D_i are given in Table III. The opposite sign is used where noted in Fig. 7. The contributions from diagrams of class IV, the bubble diagrams, are listed below. The diagrams are shown in Fig. 8. The contribution of IV.2 is identical to IV.3, that of IV.4 to IV.5 and that of IV.6 to IV.7.

$$\begin{aligned}\text{IV.1}=-3/[2^{14}\pi^{13}(k_{FC})^6]\int d\tau v(q)[v(q)-\tfrac{1}{2}v(|\mathbf{n}-\mathbf{m}-\mathbf{q}|)][v(|\mathbf{m}+\mathbf{q}+\mathbf{m}_1|)+v(|\mathbf{n}-\mathbf{q}+\mathbf{m}_1|)-v(|\mathbf{m}+\mathbf{m}_1|)\\ -v(|\mathbf{n}+\mathbf{m}_1|)]\frac{[v(|\mathbf{m}+\mathbf{q}+\mathbf{m}_2|)+v(|\mathbf{n}-\mathbf{q}+\mathbf{m}_2|-v(|\mathbf{m}+\mathbf{m}_2|)-v(|\mathbf{n}+\mathbf{m}_2|)]}{[q^2+\mathbf{q}\cdot(\mathbf{m}-\mathbf{n})]^3},\end{aligned} \tag{2.17}$$

TABLE III. Arguments of the potentials and denominators.

Diagram	x_2	x_3	D_3
III.1	q_1	$\lvert\mathbf{n}_1-\mathbf{m}-\mathbf{q}-\mathbf{q}_1\rvert$	$q^2+\mathbf{q}\cdot(\mathbf{m}-\mathbf{n})+q_1^2+\mathbf{q}_1\cdot(\mathbf{q}+\mathbf{m}-\mathbf{n}_1)$
III.2	$\lvert\mathbf{n}-\mathbf{n}_1\rvert$	$\lvert\mathbf{n}-\mathbf{m}_1\rvert$	$q^2+\mathbf{q}\cdot(\mathbf{m}-\mathbf{n})+n^2-\mathbf{n}\cdot(\mathbf{m}_1+\mathbf{n}_1)+\mathbf{n}_1\cdot\mathbf{m}_1$
III.7+8	q_1	$\lvert\mathbf{m}-\mathbf{m}_1-\mathbf{q}_1\rvert$	$q_1^2+\mathbf{q}_1\cdot(\mathbf{m}_1-\mathbf{m})$
III.9+10	$\lvert\mathbf{m}+\mathbf{q}-\mathbf{m}_1\rvert$	$\lvert\mathbf{n}_1-\mathbf{m}-\mathbf{q}\rvert$	$(\mathbf{m}+\mathbf{q})^2+\mathbf{m}_1\cdot\mathbf{n}_1-(\mathbf{m}+\mathbf{q})\cdot(\mathbf{m}_1+\mathbf{n}_1)$

$$\text{IV.2}=+3/[(2\pi)^{13}(k_FC)^6]\int d\tau v(q)v(|\mathbf{q}-\mathbf{q}_1|)[v(q_1)-\tfrac{1}{2}v(|\mathbf{q}_1+\mathbf{m}-\mathbf{n}|)]\frac{[v(|\mathbf{m}+\mathbf{q}+\mathbf{m}_1|)-v(|\mathbf{m}+\mathbf{m}_1|)]}{[q^2+\mathbf{q}\cdot(\mathbf{m}-\mathbf{n})]^2[q_1^2+\mathbf{q}_1\cdot(\mathbf{m}-\mathbf{n})]}, \quad (2.18)$$

$$\text{IV.4}=+3/[2^{12}\pi^{13}(k_FC)^6]\int d\tau\{[v(q)-\tfrac{1}{2}v(|\mathbf{n}-\mathbf{m}-\mathbf{q}|)][v(q)-\tfrac{1}{2}v(|\mathbf{n}-\mathbf{q}_1|)]$$
$$\times[v(q)-\tfrac{1}{2}v(|\mathbf{m}+\mathbf{q}-\mathbf{q}_1|)]-\tfrac{3}{8}v(|\mathbf{n}-\mathbf{m}-\mathbf{q}|)v(|\mathbf{n}-\mathbf{q}_1|)v(|\mathbf{m}+\mathbf{q}-\mathbf{q}_1|)\}$$
$$\times\frac{[v(|\mathbf{m}+\mathbf{q}+\mathbf{m}_1|)+v(|\mathbf{n}-\mathbf{q}+\mathbf{m}_1|)-v(|\mathbf{m}+\mathbf{m}_1|)-v(|\mathbf{n}+\mathbf{m}_1|)]}{[q^2+\mathbf{q}\cdot(\mathbf{m}-\mathbf{n})]^2[q^2+\mathbf{q}\cdot(\mathbf{m}-\mathbf{q}_1)]}, \quad (2.19)$$

$$\text{IV.6}=+3/[(2\pi)^{13}(k_FC)^6]\int d\tau v(q)v(|\mathbf{q}-\mathbf{q}_1|)[v(q_1)-\tfrac{1}{2}v(|\mathbf{m}-\mathbf{n}+\mathbf{q}_1|)]$$
$$\times\frac{[v(|\mathbf{m}+\mathbf{q}+\mathbf{m}_1|)-v(|\mathbf{m}+\mathbf{m}_1|)]}{[q^2+\mathbf{q}\cdot(\mathbf{m}-\mathbf{n})]^2[q^2-q_1^2+(\mathbf{q}-\mathbf{q}_1)\cdot(\mathbf{m}-\mathbf{n})]}. \quad (2.20)$$

We have now written out all the integrals which contribute to the many-body perturbation theory for a square-well force through fourth order. We shall now tabulate (Table IV) our best values for each of them, along with their standard deviation, for a selection of densities. As the number of Monte Carlo repetitions used varied from 2×10^5 to 2.8×10^6, we have used the central limit theorem to (i) show that the result obtained is normally distributed about the true answer and (ii) to estimate its standard deviation from the true result.

The diagrams which are included in the Brueckner approximation[8] through fourth order, are B1, B2, B3, F3, I.1, III.1, III.7+8, IV.1, IV.2, and IV.3.

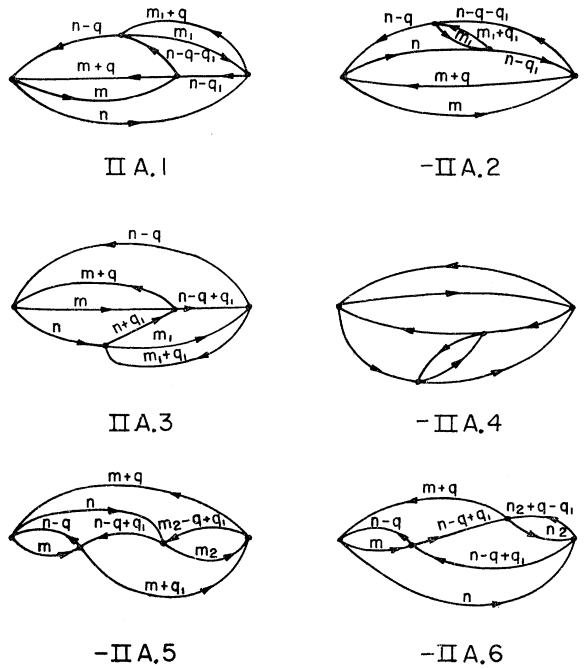

FIG. 6. Class IIA, Fourth-order perturbation theory diagrams.

[8] K. A. Brueckner, *The Many-Body Problem*, edited by C. deWitt (John Wiley & Sons, Inc., New York, 1959), pp. 65 *et seq.*

III. THE NATURE OF THE LADDER APPROXIMATION SERIES

One of the authors, (G.B.) has previously[3] shown that the ladder approximation, i.e., the sum of the ladder diagrams, B1, B2, B3, I.1, $\cdots$, is an asymptotic series whose terms increase asymptotically like $n!$ We shall show, however, that there is a unique function which is analytic in the cut plane $(-\infty,0)$ and asymptotically equal to the perturbation expansion about the origin. (This function is, of course, the one obtained from the solution of the Bethe-Goldstone equation.[9]) We will show that the Padé approximant method[2] which has been successfully applied to other physical problems[10] must converge here. In fact it can be used to obtain rigorous upper and lower bounds to the correct answer. Let v be the two-body potential operator and $1/b_i=P/(H_0-E_i)$, where H_0 is the two-body kinetic energy operator, E_i the unperturbed energy of the relevant two-body state and P a projection operator which is zero for states in the Fermi sea and one otherwise. The energy shift is then in ladder approximation

$$\Delta E=\sum_i\langle\psi_i|\left(\lambda v-v\frac{1}{b_i}v\lambda^2+v\frac{1}{b_i}v\frac{1}{b_i}v\lambda^3-v\frac{1}{b_i}v\frac{1}{b_i}v\frac{1}{b_i}v\lambda^4+\cdots\right)|\psi_i\rangle, \quad (3.1)$$

where the sum on i is over the Fermi sea and λ is regarded as an expansion parameter. Equation (3.1)

[9] H. A. Bethe and J. Goldstone, Proc. Roy. Soc. (London) **A238**, 551 (1957).

[10] G. A. Baker, Jr., Phys. Rev. **124**, 768 (1961), **129**, 99 (1963); J. L. Gammel and W. Marshall, Harwell Report, TPA-5 (1963). C. Domb and C. Isenberg, Proc. Phys. Soc. (London) **79**, 659 (1962); J. S. R. Chisholm, J. Math. Phys. (to be published). J. W. Essam and M. E. Fisher, J. Chem. Phys. **38**, 802 (1963).

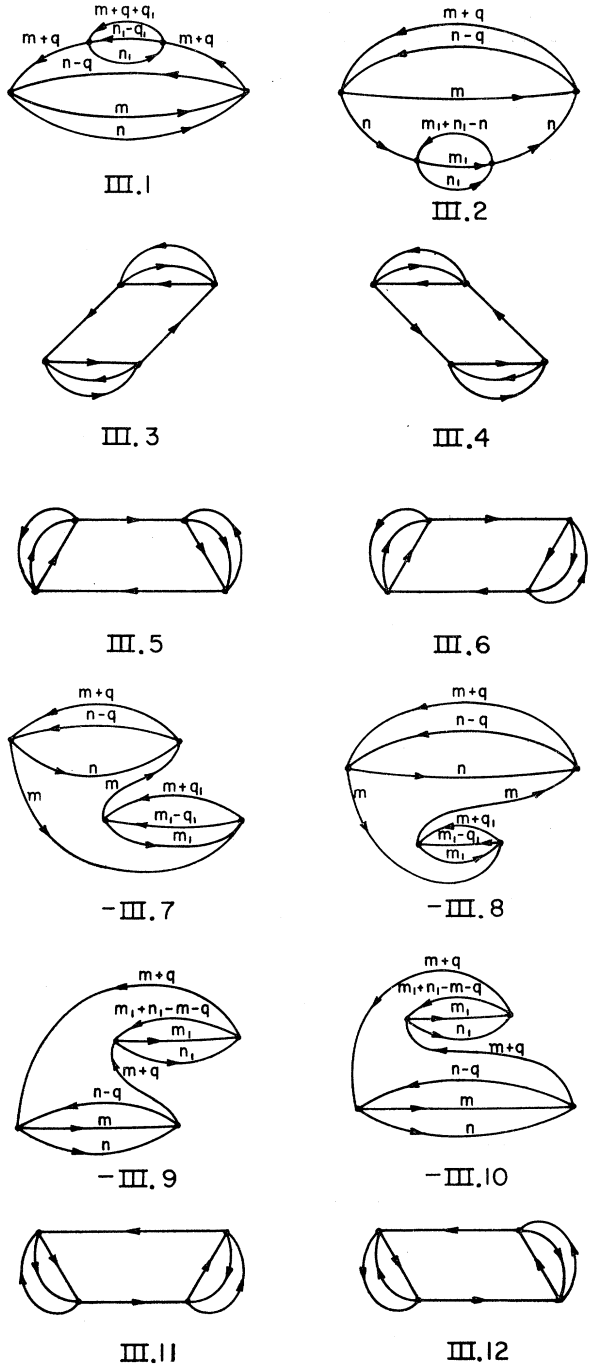

FIG. 7. Class III, Fourth-order perturbation theory diagrams.

may be rewritten as

$$\Delta E=\sum_i \langle\varphi_i|\left\{\lambda-\left(\sqrt{v}\frac{1}{b_i}\sqrt{v}\right)\lambda^2+\left(\sqrt{v}\frac{1}{b_i}\sqrt{v}\right)^2\lambda^3-\left(\sqrt{v}\frac{1}{b}\sqrt{v}\right)^3\lambda^4+\cdots\right\}|\varphi_i\rangle$$

$$=\sum\langle\varphi_i|\{\lambda+V_i\lambda^2+V_i^2\lambda^3+V_i^3\lambda^4+\cdots\}|\varphi_i\rangle, \quad (3.2)$$

where $\varphi_i=\sqrt{v}\psi_i$. Now the operator V_i is Hermitian as $1/b_i$ is Hermitian, and in coordinate representation v is greater than or equal to zero so that $\sqrt{v}$ is real and non-negative. If we now expand φ_i in a complete orthonormal set of wave functions ω_{ik} which are eigenfunctions of V_i with real eigenvalues V_{ik}, Eq. (3.2) becomes

$$\Delta E=\sum_i\left[\sum_k\{\lambda-V_{ik}\lambda^2+V_{ik}^2\lambda^3-V_{ik}^3\lambda^4+\cdots\}\times|a_{ik}|^2\right]. \quad (3.3)$$

Since $|a_{ik}|^2\geq 0$ and by the normalization of the original

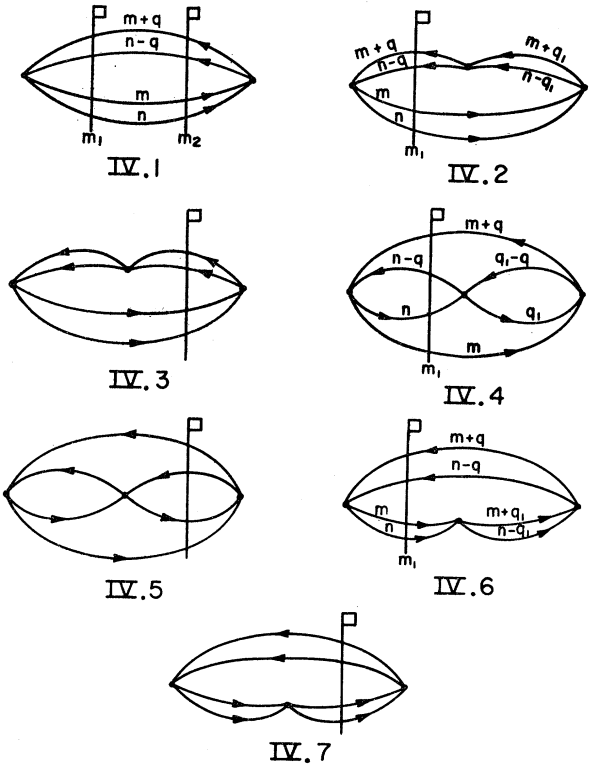

FIG. 8. Class IV, Fourth-order perturbation theory diagrams.

wave function, the expected value of v is finite

$$\sum_i\langle\psi_i|v|\psi_i\rangle=\sum_{i,k}|a_{ik}|^2, \quad (3.4)$$

and if we denote by $(-1)^p c_p$ the term from the coefficient of the $(p+1)$st power of λ, then there exists a bounded, nondecreasing function $\varphi(u)$, such that

$$c_p=\int_{-\infty}^{+\infty}u^p d\varphi(u). \quad (3.5)$$

The function φ will take on infinitely many values if and only if there are infinitely many eigenvalues involved. According to Theorem 86.1 of Wall[11] Eq. (3.5)

[11] H. S. Wall, *Analytic Theory of Continued Fractions* (D. Van Nostrand Company, New York, 1948), Chap. XVII.

TABLE IV. Monte Carlo calculations.

Diagram	$k_{FC}=0.25$ Value	Deviation	$k_{FC}=0.50$ Value	Deviation	$k_{FC}=0.75$ Value	Deviation
B1[b]	5.567499×10^{-4}	...	4.551588×10^{-3}	...	1.589397×10^{-2}	...
B2[b]	-1.960×10^{-4}	1.2×10^{-6}	-1.346×10^{-3}	2.4×10^{-6}	-3.827×10^{-3}	4.6×10^{-6}
B3[b]	7.003×10^{-5}	5.7×10^{-7}	4.146×10^{-4}	1.7×10^{-6}	9.742×10^{-4}	3.1×10^{-6}
H3	1.75×10^{-7}	1.6×10^{-9}	4.45×10^{-6}	4.3×10^{-8}	2.57×10^{-5}	2.0×10^{-7}
R3	-8.60×10^{-7}	6.8×10^{-9}	-2.14×10^{-5}	1.6×10^{-7}	-1.175×10^{-4}	6.4×10^{-7}
F3[b]	3.95×10^{-8}	2.3×10^{-10}	2.10×10^{-6}	5.0×10^{-8}	1.89×10^{-5}	2.5×10^{-7}
Σ3	6.939×10^{-5}	5.7×10^{-7}	4.00×10^{-4}	1.7×10^{-6}	9.013×10^{-4}	3.2×10^{-6}
ΣB3	7.007×10^{-5}	5.7×10^{-7}	4.167×10^{-4}	1.7×10^{-6}	9.931×10^{-4}	3.1×10^{-6}
I.1[b]	-2.506×10^{-5}	1.9×10^{-7}	-1.288×10^{-4}	4.4×10^{-7}	-2.571×10^{-4}	1.1×10^{-6}
I.2	-6.30×10^{-8}	6.1×10^{-10}	-1.36×10^{-6}	5.0×10^{-8}	-6.82×10^{-6}	1.5×10^{-7}
I.3+4	-6.22×10^{-8}	6.0×10^{-10}	-1.41×10^{-6}	4.5×10^{-8}	-7.10×10^{-6}	9.4×10^{-8}
I.5[a]	-6.30×10^{-8}	6.1×10^{-10}	-1.36×10^{-6}	5.0×10^{-8}	-6.82×10^{-6}	1.5×10^{-7}
I.6	-9.93×10^{-10}	1.8×10^{-11}	-5.58×10^{-8}	9.5×10^{-10}	-5.16×10^{-7}	8.6×10^{-9}
I-A.1	-1.01×10^{-8}	2.9×10^{-10}	-5.36×10^{-7}	1.6×10^{-8}	-4.68×10^{-6}	1.4×10^{-7}
I-A.2	-4.65×10^{-9}	1.8×10^{-10}	-2.40×10^{-7}	8.4×10^{-9}	-2.00×10^{-6}	6.0×10^{-8}
I-A.3	-9.39×10^{-9}	1.5×10^{-10}	-4.94×10^{-7}	7.2×10^{-9}	-4.24×10^{-6}	5.8×10^{-8}
II.1	3.07×10^{-7}	3.1×10^{-9}	6.71×10^{-6}	1.0×10^{-7}	3.15×10^{-5}	2.2×10^{-7}
II.2[a]	3.07×10^{-7}	3.1×10^{-9}	6.71×10^{-6}	1.0×10^{-7}	3.15×10^{-5}	2.2×10^{-7}
II.3	2.45×10^{-9}	4.3×10^{-11}	1.38×10^{-7}	2.1×10^{-9}	1.26×10^{-6}	1.7×10^{-8}
II.4[a]	2.45×10^{-9}	4.3×10^{-11}	1.38×10^{-7}	2.1×10^{-9}	1.26×10^{-6}	1.7×10^{-8}
II.5	9.00×10^{-8}	4.5×10^{-10}	2.72×10^{-6}	1.0×10^{-7}	1.39×10^{-5}	1.9×10^{-7}
II.6	2.28×10^{-7}	1.5×10^{-9}	4.22×10^{-6}	9.5×10^{-8}	1.86×10^{-5}	2.9×10^{-7}
II.7	-2.77×10^{-9}	2.3×10^{-11}	-1.46×10^{-7}	1.2×10^{-9}	-1.20×10^{-6}	1.0×10^{-8}
II.8	-4.66×10^{-9}	1.7×10^{-10}	-1.96×10^{-7}	3.7×10^{-9}	-1.34×10^{-6}	1.8×10^{-8}
II.9	1.45×10^{-9}	3.3×10^{-11}	8.06×10^{-8}	1.5×10^{-9}	7.34×10^{-7}	1.3×10^{-8}
II.10	5.04×10^{-10}	1.3×10^{-11}	2.92×10^{-8}	7.2×10^{-10}	2.80×10^{-7}	7.0×10^{-9}
II.11[a]	-4.66×10^{-9}	1.7×10^{-10}	-1.96×10^{-7}	3.7×10^{-9}	-1.34×10^{-6}	1.8×10^{-8}
II.12[a]	-2.77×10^{-9}	2.3×10^{-11}	-1.46×10^{-7}	1.2×10^{-9}	-1.20×10^{-6}	1.0×10^{-8}
II-A.1	-9.12×10^{-8}	4.6×10^{-10}	-2.80×10^{-6}	3.7×10^{-8}	-1.68×10^{-5}	1.7×10^{-7}
II-A.2	$+4.94\times10^{-9}$	1.2×10^{-10}	2.84×10^{-7}	6.6×10^{-9}	2.73×10^{-6}	6.3×10^{-8}
II-A.3	-6.88×10^{-10}	1.0×10^{-11}	-4.26×10^{-8}	6.2×10^{-10}	-4.57×10^{-7}	6.7×10^{-9}
II-A.4[a]	4.94×10^{-9}	1.2×10^{-10}	2.84×10^{-7}	6.6×10^{-9}	2.73×10^{-6}	6.3×10^{-8}
II-A.5	4.74×10^{-9}	4.7×10^{-11}	2.22×10^{-7}	2.1×10^{-9}	1.64×10^{-6}	1.9×10^{-8}
II-A.6	4.41×10^{-9}	6.3×10^{-11}	2.11×10^{-7}	2.9×10^{-9}	1.65×10^{-6}	2.5×10^{-8}
III.1[b]	-3.01×10^{-7}	2.1×10^{-9}	-6.13×10^{-6}	9.7×10^{-8}	-3.01×10^{-5}	2.8×10^{-7}
III.2	-4.59×10^{-9}	5.9×10^{-11}	-2.54×10^{-7}	3.0×10^{-9}	-2.31×10^{-6}	2.7×10^{-8}
III.7+8[b]	3.66×10^{-7}	1.6×10^{-9}	8.28×10^{-6}	1.2×10^{-7}	4.21×10^{-5}	3.0×10^{-7}
III.9+10	6.86×10^{-9}	2.0×10^{-10}	3.67×10^{-7}	9.3×10^{-9}	3.15×10^{-6}	6.5×10^{-8}
IV.1[b]	-6.2×10^{-12}	1.0×10^{-12}	-3.46×10^{-9}	3.3×10^{-10}	-9.75×10^{-8}	3.8×10^{-9}
IV.2[b]	-1.35×10^{-8}	4.9×10^{-10}	-6.79×10^{-7}	4.5×10^{-8}	-4.62×10^{-6}	1.4×10^{-7}
IV.3[b]	-1.35×10^{-8}	4.9×10^{-10}	-6.79×10^{-7}	4.5×10^{-8}	-4.62×10^{-6}	1.4×10^{-7}
IV.4	1.83×10^{-10}	9.8×10^{-12}	3.60×10^{-8}	1.2×10^{-9}	6.15×10^{-7}	1.0×10^{-8}
IV.5[a]	1.83×10^{-10}	9.8×10^{-12}	3.60×10^{-8}	1.2×10^{-9}	6.15×10^{-7}	1.0×10^{-8}
IV.6	3.90×10^{-11}	3.2×10^{-12}	7.70×10^{-9}	3.6×10^{-10}	1.40×10^{-7}	3.9×10^{-9}
IV.7[a]	3.90×10^{-11}	3.2×10^{-12}	7.70×10^{-9}	3.6×10^{-10}	1.40×10^{-7}	3.9×10^{-9}
Σ4	-2.438×10^{-5}	1.9×10^{-7}	-1.149×10^{-4}	5.5×10^{-7}	-1.989×10^{-4}	1.4×10^{-6}
ΣB4	-2.509×10^{-5}	1.9×10^{-7}	-1.280×10^{-4}	4.8×10^{-7}	-2.544×10^{-4}	1.2×10^{-6}

Diagram	$k_{FC}=1.0$ Value	Deviation	$k_{FC}=1.5$ Value	Deviation
B1[b]	3.936174×10^{-2}	...	1.475170×10^{-1}	...
B2[b]	-7.495×10^{-3}	1.9×10^{-5}	-1.715×10^{-2}	4.8×10^{-5}
B3[b]	1.538×10^{-3}	5.0×10^{-6}	2.190×10^{-3}	1.1×10^{-5}
H3	7.87×10^{-5}	5.6×10^{-7}	2.81×10^{-4}	2.2×10^{-6}
R3	-3.30×10^{-4}	1.7×10^{-6}	-7.98×10^{-4}	7.7×10^{-6}
F3[b]	8.08×10^{-5}	8.3×10^{-7}	5.05×10^{-4}	4.6×10^{-6}
Σ3	1.368×10^{-3}	5.3×10^{-6}	2.178×10^{-3}	1.4×10^{-5}
ΣB3	1.619×10^{-3}	5.1×10^{-6}	2.695×10^{-3}	1.2×10^{-5}
I.1[b]	-3.347×10^{-4}	2.1×10^{-6}	-3.01×10^{-4}	4.7×10^{-6}
I.2	-1.75×10^{-5}	3.4×10^{-7}	-3.93×10^{-5}	6.6×10^{-7}
I.3+4	-1.85×10^{-5}	3.4×10^{-7}	-4.51×10^{-5}	6.8×10^{-7}
I.5[a]	-1.75×10^{-5}	3.4×10^{-7}	-3.93×10^{-5}	6.6×10^{-7}
I.6	-2.19×10^{-6}	3.7×10^{-8}	-1.16×10^{-5}	2.3×10^{-7}
I-A.1	-1.89×10^{-5}	5.4×10^{-7}	-1.01×10^{-4}	1.0×10^{-6}
I-A.2	-7.82×10^{-6}	2.2×10^{-7}	-4.56×10^{-4}	8.8×10^{-7}
I-A.3	-1.67×10^{-5}	2.4×10^{-7}	-8.50×10^{-5}	8.4×10^{-7}
II.1	7.40×10^{-5}	4.8×10^{-7}	1.20×10^{-4}	1.2×10^{-6}
II.2[a]	7.40×10^{-5}	4.8×10^{-7}	1.20×10^{-4}	1.2×10^{-6}
II.3	5.23×10^{-6}	7.0×10^{-8}	2.39×10^{-5}	3.3×10^{-7}
II.4[a]	5.23×10^{-6}	7.0×10^{-8}	2.39×10^{-5}	3.3×10^{-7}
II.5	3.42×10^{-5}	3.9×10^{-7}	4.76×10^{-5}	9.5×10^{-7}
II.6	4.18×10^{-5}	5.4×10^{-7}	5.85×10^{-5}	1.4×10^{-6}
II.7	-4.23×10^{-6}	2.9×10^{-8}	-1.06×10^{-5}	2.1×10^{-7}

TABLE IV (*continued*)

Diagram	$k_{FC}=1.0$ Value	$k_{FC}=1.0$ Deviation	$k_{FC}=1.5$ Value	$k_{FC}=1.5$ Deviation
II.8	-4.00×10^{-6}	6.6×10^{-8}	-6.23×10^{-6}	3.9×10^{-7}
II.9	3.02×10^{-6}	5.5×10^{-8}	1.33×10^{-5}	2.7×10^{-7}
II.10	1.22×10^{-6}	3.2×10^{-8}	6.38×10^{-6}	1.7×10^{-7}
II.11[a]	-4.00×10^{-6}	6.6×10^{-8}	-6.32×10^{-6}	3.9×10^{-7}
II.12[a]	-4.23×10^{-6}	2.9×10^{-8}	-1.06×10^{-5}	2.1×10^{-7}
II-A.1	-5.21×10^{-5}	5.4×10^{-7}	-2.17×10^{-4}	9.8×10^{-7}
II-A.2	1.24×10^{-5}	2.9×10^{-7}	8.41×10^{-5}	1.7×10^{-6}
II-A.3	-2.35×10^{-6}	3.6×10^{-8}	-2.03×10^{-5}	2.8×10^{-7}
II-A.4[a]	1.24×10^{-5}	2.9×10^{-7}	8.41×10^{-5}	1.7×10^{-6}
II-A.5	5.62×10^{-6}	9.1×10^{-8}	3.12×10^{-5}	5.7×10^{-7}
II-A.6	6.31×10^{-6}	1.2×10^{-7}	4.01×10^{-5}	7.8×10^{-7}
III.1[b]	-8.32×10^{-5}	5.3×10^{-7}	-2.78×10^{-4}	1.8×10^{-6}
III.2	-9.81×10^{-6}	1.3×10^{-7}	-5.69×10^{-5}	8.0×10^{-7}
III.7+8[b]	1.155×10^{-4}	6.7×10^{-7}	3.68×10^{-4}	2.9×10^{-6}
III.9+10	1.24×10^{-5}	1.6×10^{-7}	6.53×10^{-5}	6.4×10^{-7}
IV.1[b]	-9.08×10^{-7}	2.2×10^{-8}	-1.55×10^{-5}	1.7×10^{-7}
IV.2[b]	-1.65×10^{-5}	3.7×10^{-7}	-6.42×10^{-5}	8.9×10^{-7}
IV.3[ab]	-1.65×10^{-5}	3.7×10^{-7}	-6.42×10^{-5}	8.9×10^{-7}
IV.4	3.74×10^{-6}	4.7×10^{-8}	2.47×10^{-5}	3.4×10^{-7}
IV.5[a]	3.74×10^{-6}	4.7×10^{-8}	2.47×10^{-5}	3.4×10^{-7}
IV.6	9.42×10^{-7}	2.4×10^{-8}	9.36×10^{-6}	1.9×10^{-7}
IV.7[a]	9.42×10^{-7}	2.4×10^{-8}	9.36×10^{-6}	1.9×10^{-7}
Σ4	-2.19×10^{-4}	2.9×10^{-6}	-2.64×10^{-4}	8.2×10^{-6}
ΣB4	-3.363×10^{-4}	2.4×10^{-6}	-3.55×10^{-4}	6.1×10^{-6}

Diagram	$k_{FC}=2.0$ Value	$k_{FC}=2.0$ Deviation	$k_{FC}=3.0$ Value	$k_{FC}=3.0$ Deviation
B1[b]	3.901006×10^{-1}	...	1.574696×10^{0}	...
B2[b]	-2.868×10^{-2}	5.9×10^{-5}	-5.367×10^{-2}	3.3×10^{-4}
B3[b]	2.44×10^{-3}	2.0×10^{-5}	2.73×10^{-3}	1.2×10^{-4}
H3	4.99×10^{-4}	5.7×10^{-6}	8.21×10^{-4}	2.1×10^{-5}
R3	-2.61×10^{-4}	1.3×10^{-5}	$+4.75\times10^{-3}$	2.0×10^{-4}
F3[b]	1.51×10^{-3}	1.5×10^{-5}	4.45×10^{-3}	6.6×10^{-5}
Σ3	4.19×10^{-3}	2.9×10^{-5}	1.275×10^{-2}	2.4×10^{-4}
ΣB3	3.95×10^{-3}	2.5×10^{-5}	7.18×10^{-3}	1.4×10^{-4}
I.1[b]	-2.25×10^{-4}	9.4×10^{-6}	-1.09×10^{-4}	2.8×10^{-5}
I.2	-4.13×10^{-5}	1.4×10^{-6}	-3.54×10^{-5}	4.6×10^{-6}
I.3+4	-4.69×10^{-5}	1.3×10^{-6}	-2.71×10^{-5}	4.0×10^{-6}
I.5[a]	-4.13×10^{-5}	1.4×10^{-6}	-3.54×10^{-5}	4.6×10^{-6}
I.6	-2.39×10^{-5}	7.0×10^{-7}	-2.82×10^{-5}	2.0×10^{-6}
I-A.1	-2.80×10^{-4}	5.2×10^{-6}	-1.35×10^{-3}	8.4×10^{-5}
I-A.2	-1.77×10^{-4}	2.6×10^{-6}	-1.06×10^{-3}	5.6×10^{-5}
I-A.3	-2.32×10^{-4}	3.2×10^{-6}	-1.30×10^{-3}	1.2×10^{-4}
II.1	1.98×10^{-5}	3.9×10^{-6}	-2.46×10^{-4}	3.2×10^{-5}
II.2[a]	1.98×10^{-5}	3.9×10^{-6}	-2.46×10^{-4}	3.2×10^{-5}
II.3	2.86×10^{-5}	1.4×10^{-6}	-1.00×10^{-4}	1.3×10^{-5}
II.4[a]	2.86×10^{-5}	1.4×10^{-6}	-1.00×10^{-4}	1.3×10^{-5}
II.5	-3.51×10^{-5}	2.7×10^{-6}	-2.39×10^{-4}	3.3×10^{-5}
II.6	-1.67×10^{-5}	4.0×10^{-6}	-2.36×10^{-4}	4.2×10^{-5}
II.7	$+1.05\times10^{-5}$	1.1×10^{-6}	1.36×10^{-4}	1.1×10^{-5}
II.8	$+1.92\times10^{-5}$	1.8×10^{-6}	1.38×10^{-4}	1.2×10^{-5}
II.9	1.29×10^{-5}	1.1×10^{-6}	-9.71×10^{-5}	9.7×10^{-6}
II.10	8.46×10^{-6}	7.4×10^{-7}	-3.51×10^{-5}	6.7×10^{-6}
II.11[a]	$+1.92\times10^{-5}$	1.8×10^{-6}	1.38×10^{-4}	1.2×10^{-5}
II.12[a]	$+1.05\times10^{-5}$	1.1×10^{-6}	1.36×10^{-4}	1.1×10^{-5}
II-A.1	-5.28×10^{-4}	3.6×10^{-6}	-1.228×10^{-3}	5.3×10^{-5}
II-A.2	2.86×10^{-4}	8.8×10^{-6}	1.258×10^{-3}	6.6×10^{-5}
II-A.3	-7.87×10^{-5}	1.5×10^{-6}	-3.76×10^{-4}	1.5×10^{-5}
II-A.4[a]	2.86×10^{-4}	8.8×10^{-6}	1.258×10^{-3}	6.6×10^{-5}
II-A.5	1.39×10^{-4}	2.1×10^{-6}	6.85×10^{-4}	2.3×10^{-5}
II-A.6	1.54×10^{-4}	2.0×10^{-6}	6.92×10^{-4}	3.3×10^{-5}
III.1[b]	-5.75×10^{-4}	5.7×10^{-6}	-1.248×10^{-3}	6.5×10^{-5}
III.2	-1.71×10^{-4}	3.7×10^{-6}	-5.92×10^{-4}	3.1×10^{-5}
III.7+8[b]	7.36×10^{-4}	1.0×10^{-5}	1.568×10^{-3}	6.5×10^{-5}
III.9+10	1.80×10^{-4}	2.4×10^{-6}	6.71×10^{-4}	3.3×10^{-5}
IV.1[b]	-8.43×10^{-5}	8.8×10^{-7}	-3.90×10^{-4}	7.7×10^{-6}
IV.2[b]	-1.32×10^{-4}	2.6×10^{-6}	-2.67×10^{-4}	4.6×10^{-5}
IV.3[ab]	-1.32×10^{-4}	2.6×10^{-6}	-2.67×10^{-4}	4.6×10^{-5}
IV.4	1.21×10^{-5}	1.8×10^{-6}	-4.86×10^{-4}	3.3×10^{-5}
IV.5[a]	1.21×10^{-5}	1.8×10^{-6}	-4.86×10^{-4}	3.3×10^{-5}
IV.6	3.12×10^{-5}	8.4×10^{-7}	8.95×10^{-5}	5.5×10^{-6}
IV.7[a]	3.12×10^{-5}	8.4×10^{-7}	8.95×10^{-5}	5.5×10^{-6}
Σ4	-7.75×10^{-4}	2.8×10^{-5}	-3.73×10^{-3}	2.6×10^{-4}
ΣB4	-4.12×10^{-4}	1.6×10^{-5}	-7.13×10^{-4}	1.3×10^{-4}

[a] Identical with a previous diagram (but must be added to find the total fourth-order coefficient).
[b] Included in the Brueckner approximation.

is necessary and sufficient that

$$\Delta_p=\begin{vmatrix} c_0 & c_1, & \cdots, & c_p \\ c_1, & c_2, & \cdots, & c_{p+1} \\ \vdots & & & \\ c_p, & c_{p+1}, & \cdots, & c_{2p} \end{vmatrix} >0 \quad p=0,1,2,\cdots, \quad (3.6)$$

except if only a finite number of eigenvalues occur all $\Delta_p=0$ for $p\geq P$. If we now define the Hermitian operator $w_i=(1/\sqrt{b_i})v(1/\sqrt{b_i})$ and define $\varphi_i=(1/\sqrt{b_i})\times v\psi_i$, then a similar argument implies that

$$\Omega_p=\begin{vmatrix} c_1 & c_2, & \cdots, & c_{p+1} \\ c_2 & c_3, & \cdots, & c_{p+2} \\ \vdots & & & \\ c_{p+1}, & c_{p+2}, & \cdots, & c_{2p+1} \end{vmatrix} >0$$

$$p=0,1,2,\cdots, \quad (3.7)$$

except again where there are only a finite number of eigenvalues. According to Wall's theorem 87.1, Eqs. (3.6) and (3.7) are necessary and sufficient that the c_p form a series of Stieljes, and hence that

$$c_p=\int_0^{+\infty} u^p d\varphi(u). \quad (3.8)$$

As the coefficients only diverge[3] like $n!$ we are dealing (Theorem 88.1)[11] with the case of a unique φ. Hence, the diagonal Padé approximants converge to the unique function

$$\Delta E(\lambda)=\int_0^{\infty} \frac{\lambda d\varphi(u)}{1+u\lambda}, \quad (3.9)$$

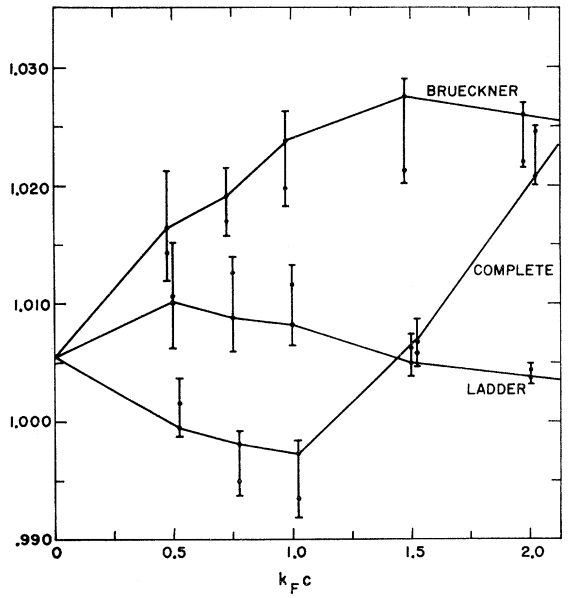

FIG. 9. Comparison of the ladder approximation, the Brueckner approximation, and the complete perturbation theory for $V=2.5$ as represented by the [1,2] and [2,2] Padé approximants. For convenient presentation the results have been normalized by dividing by the [1,1] Padé approximant.

defined by the perturbation series. The Padé approximants $[N,M]$ are the ratio of two polynomials $P_M(\lambda)/Q_N(\lambda)$ determined so as to match the first $M+N+1$ coefficients of λ^n in the $[Q_N(0)=1.0]$ power-series expansion. Furthermore, according to Wall's problem 17.3,[11] the sequence of $[N,N]$ Padé approximants are less than (3.9) for all real positive λ and the $[N,N+1]$ are all greater for real positive λ. We will use this result in a subsequent section to bound the true result and to compare with results of the solution of the ladder approximation integral equation obtained with the usual approximations.

It should be noted that these bounds are the best obtainable when only the information concerning the specific potential contained in the coefficients used to form the approximants is considered. This result is so because there exist (velocity-dependent) potentials for which the relevant Padé approximant is an exact answer; namely, they belong to the class of potentials which are diagonal in the momentum representation and couple only N-momentum states. Even so, the covergence at the hard-core limit ($\lambda=+\infty$) may be relatively slow[2] for asymptotic series.

IV. COMPARISON OF THE RESULTS OF THE LADDER AND BRUECKNER APPROXIMATIONS FOR SOFT REPULSIVE SQUARE-WELL POTENTIALS

On the basis of the perturbation theory coefficients obtained in Sec. II, we may, as shown in Sec. III, for various values of the strength V, give upper and lower bounds for the ladder approximation. That is, it must lie between the [2,2] and the [1,2] Padé approximants. We shall assume that for the complete theory and the Brueckner approximation that, while the approximants may not bound the function values, the difference between the [2,2] and the [1,2] gives a measure of accuracy of the [2,2] and that where the difference between the theories as indicated by the [2,2] is large compared to the apparent error in the [2,2], the ordering of the theories is correctly given. For sample potential values we have chosen $(VMc^2/\hbar^2)=2.5$ and 5.0. These correspond to slightly less and slightly more than a half-hard core (in terms of the scattering length).

In Figs. 9 and 10, we have, for convenience, plotted the ratio of the [1,2] and [2,2] to the [1,1] (the [1,1] approximant is the same for the ladder approximation, the Brueckner approximation, and the complete perturbation series).

The points represent the values of the approximants. The [2,2] are joined by lines and the different theories are slightly offset for clarity. The flags represent statistical uncertainty in the values of the approximants due to inaccuracies in the calculation of the coefficients.

We see that at low densities the complete theory lies below the ladder approximation while the Brueckner approximation lies above it. The reason that the Brueckner approximation is less accurate than the

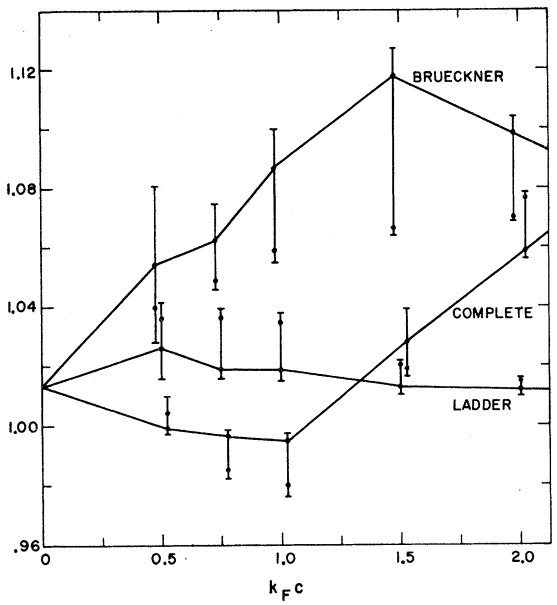

FIG. 10. Comparison of the ladder approximation, the Brueckner approximation, and the complete perturbation theory for $V=5.0$ as represented by the [1,2] and [2,2] Padé approximants. For convenient presentation the results have been normalized by dividing by the [1,1] Padé approximant.

ladder can easily be seen by looking at the third order terms. The first low-density corrections to the ladder diagram B3, is the ring diagram R3 and the hole-hole interaction diagram H3. These terms are proportional to $(k_F c)^5$. Brueckner includes diagram F3 which is proportional to $(k_F c)^6$ and has the opposite sign from R3. The same trouble also occurs in fourth order where the leading order corrections are given by II.1, II.2, II.6, and I.3+4 which are proportional to $(k_F c)^5$ (III.1, III.7+8, II.5 and IIA.1 cancel in pairs). Brueckner again includes only corrections proportional to $(k_F c)^6$. We estimate that for a hard core, the difference between the theories must be at least 10–20%. It is hard to assess the differences between the theories when both attraction and repulsion are present, but we know of no reasons not to suppose that they are substantial.

The rigorous upper and lower bounds which we obtained for the ladder approximation allow us to assess the accuracy of the standard solution procedures which we describe in detail in the next section. Comparison reveals that the accuracy of the standard solution is reasonably uniform in density ($0.25 \leq k_F c \leq 3.0$). The solution obtained is about 0.5% high for small V ($V \ll 1$). As V increases to around 5 the solution rises to become about 1 to $2\frac{1}{2}$% high as $k_F c$ varies from 0.25 to 3.0. At larger potentials the standard solution lies between the upper and lower bounds so no firm conclusion can be drawn about the accuracy. For infinite V ($V=10^5$) the lower bound drops ($k_F c \gtrsim 0.75$) to about two-thirds of the standard solution. At $k_F c=0$ the lower bound is 14/15 of the exact answer. From a consideration of the way in which errors occur in the standard solution, we feel that even at infinite potential it is probably not worse than about 10% high and that it has a reasonably consistent bias.

That the Padé approximants to the ladder approximation should be so relatively low for the hard-core limit is somewhat disappointing; however, the reasons are fairly clear. As pointed out above, the Padé approximants converge more slowly for asymptotic series than they do for convergent ones. Furthermore, the point $V=\infty$ is a singularity of the function, and the convergence of the sequence of Padé approximants is frequently much slower at singular points than at regular points. For instance, a somewhat analogous case, $[1-x^{-1}\ln(1+x)]$, is of the form of Eq. (3.9). Luke[12] has shown that for $0 \leq x < \infty$ the convergence of the $[N,N]$ Padé approximants is exponential. Yet at $x=+\infty$ the error in the $[N,N]$ is $(N+1)^{-2}$.

As we will explain in the next section, the numerical solution for the Brueckner approximation is not strictly comparable with the results obtained from the inferred power series expansion. The additional computational approximation introduced, in contrast to those also used in the solution of the ladder approximation integral equation, is rather poor. Consequently, while the expected departures from the ladder theory as shown in Figs. 9 and 10 occur for weak potentials, at large potentials the "as practiced" Brueckner approximation lies only slightly above that of the ladder approximation and actually crosses below it near $k_F c=1.5$. By the time the Brueckner approximation ceases to exist near $k_F c=2.0$, it is (for $V=10^5$) only about two-thirds as large as the ladder approximation.

V. THE BRUECKNER THEORY AS ORDINARILY CALCULATED

A rigorous formulation of the K-matrix equation, including off-energy shell effects correctly, is set forth in Appendix A of Brueckner and Gammel.[13] In order to carry out calculations, it is usual to eliminate the dependence of the K matrices on the total momentum by making the following approximations. An energy denominator D

$$D=E(\tfrac{1}{2}\mathbf{p}+\mathbf{k}')+E(\tfrac{1}{2}\mathbf{p}-\mathbf{k}') -E(\tfrac{1}{2}\mathbf{p}+\mathbf{k})-E(\tfrac{1}{2}\mathbf{p}-\mathbf{k}), \quad (5.1)$$

where $\mathbf{p}$ is the total momentum, $\mathbf{k}$ is the relative momentum in the initial state, and $\mathbf{k}'$ the relative momentum in the intermediate state (an integration variable in the K-matrix equations), is set equal to

$$D=2[E(k')-E(k)]. \quad (5.2)$$

This is correct if the E's are approximately quadratic

[12] Y. L. Luke, J. Math. and Phys. **37**, 110 (1958).
[13] K. A. Brueckner and J. L. Gammel, Phys. Rev. **109**, 1023 (1958).

functions of their argument. The Pauli principle requires that the integration over $\mathbf{k}'$ be restricted to a region R such that

$$|\tfrac{1}{2}\mathbf{p}+\mathbf{k}'|>k_F \quad \text{and} \quad |\tfrac{1}{2}\mathbf{p}-\mathbf{k}'|>k_F \quad \text{in } R. \tag{5.3}$$

This is approximated by replacing

$$\int_R d\mathbf{k}' \rightarrow \int d\mathbf{k}' F(p,k',k), \tag{5.4}$$

where

$$\begin{aligned} F(p,k',k)&=0, \ (k'^2+\tfrac{1}{4}p^2)^{1/2}<k_F \\ &=1, \ k'-\tfrac{1}{2}p \quad\ >k_F \\ &\quad \frac{k'^2+\frac{1}{4}p^2-k_F^2}{k'p}, \quad \text{otherwise.} \end{aligned} \tag{5.5}$$

To eliminate $\mathbf{p}$ completely, an average value $\bar{p}$ is used in place of p:

$$\begin{aligned} \tfrac{1}{4}\bar{p}^2&=\tfrac{3}{5}k_F^2\left(1-\frac{k}{k_F}\right)\frac{1+\frac{1}{2}\frac{k}{k_F}+\frac{1}{6}\frac{k^2}{k_F^2}}{1+\frac{1}{2}\frac{k}{k_F}} \quad k<k_F \\ &=0 \qquad\qquad\qquad\qquad\qquad\qquad k>k_F. \end{aligned} \tag{5.6}$$

The off-energy shell effects have to be approximated also [the K matrices and single-particle energies depend on a variable H according to Brueckner and Gammel, Appendix A; we have already suppressed this fact in writing Eq. (5.1)]; eventually the following set of equations, which are the same as the equations used by Brueckner and Masterson in their recent work[14] are arrived at, after transforming the equations to coordinate space, as done in Refs. 13 and 14. The Green's function is

$$G_{kl}(r,r')=\int_0^\infty k''^2 dk'' \frac{j_l(k''r)j_l(k''r')}{2[E(k'')-\Delta(k)]}F(\bar{p},k'',k), \tag{5.7}$$

where j is a radial Bessel function, l is the angular momentum, and

$$\begin{aligned} \Delta(k)&=E(k) \qquad\qquad\qquad\qquad k<k_F \\ &=E(k_F)-f[E(k_F)-E(0)] \quad k\geq k_F, \end{aligned} \tag{5.8}$$

where f is chosen arbitrarily. It is in the definition of $\Delta(k)$ that approximations to off-energy shell effects manifest themselves. Continuing with the equations, the wave function u satisfies the integral equation

$$u_{kl}(r)=j_l(kr)-\frac{2}{\pi}\int_0^\infty G_{kl}(r,r')V(r')u_{kl}(r')r'^2dr', \tag{5.9}$$

where V is the potential. The K matrices are given by

$$K_l(k)=\frac{2}{\pi}\int_0^\infty j_l(kr)V(r)u_{kl}(r)r^2dr, \tag{5.10}$$

and the single-particle energies by

$$\begin{aligned} E(m)&=\frac{m^2}{2}+4\left[\int_0^{(k_F-m)/2} 2k^2dkI \right. \\ &\quad \left. +\int_{(k_F-m)/2}^{(k_F+m)/2}\left(1-\frac{m^2+4k^2-k_F^2}{4km}\right)k^2dkI\right] \\ &\qquad\qquad\qquad\qquad\qquad\qquad m<k_F \\ &=\frac{m^2}{2}+4\left[\int_{(m-k_F)/2}^{(m+k_F)/2}\left(1-\frac{m^2+4k^2-k_F^2}{4km}\right)k^2dkI\right] \\ &\qquad\qquad\qquad\qquad\qquad\qquad m\geq k_F, \end{aligned} \tag{5.11}$$

where

$$I=\sum_l (2l+1)\begin{pmatrix}1 \ l \text{ even}\\ 3 \ l \text{ odd}\end{pmatrix}K_l(k). \tag{5.12}$$

Finally, the average binding energy per particle is

$$E_b=\frac{3}{2k_F^3}\int_0^{k_F}\left(E(m)-\frac{m^2}{2}\right)m^2dm. \tag{5.13}$$

Perhaps the only point worth commenting on is the origin of complicated factors in Eq. (5.11); the expected equation is

$$E(m)=\frac{m^2}{2}+\frac{2}{(2\pi)^3}\int d\mathbf{n}[(\mathbf{m}\,\mathbf{n}|K|\mathbf{m}\,\mathbf{n})-\tfrac{1}{2}K_{\text{exchange}}]. \tag{5.14}$$

Instead of $\mathbf{n}$, the variable $\mathbf{k}=\frac{1}{2}(\mathbf{m}-\mathbf{n})$ has been used, and the requirement $n<k_F$, and an integration over the angles of $\mathbf{k}$, results in the factors.

We are not interested in the details of these equations, or the techniques used in solving them, which have been discussed at length in Refs. 13 and 14. A few details of our computational procedure follow: In calculating the Green's function [Eq. (5.7)] we used an interval size $\Delta k''=0.1k_F$, and did a Simpson's rule integration to $k''=10k_F$. For the contribution ΔG from $10k_F$ to ∞, we used an asymptotic expression

$$\begin{aligned} F(y)&=\cos y\frac{1+\left(\frac{\pi^2}{20}-\frac{1}{3}\right)y^2}{1+\frac{\pi}{2}y+\left(\frac{3}{10}\pi^2-\frac{3}{2}\right)y^2+\left(\frac{1}{40}\pi^2-\frac{1}{6}\right)y^4} \\ &\quad -\frac{y}{6+y}\sin y \\ \Delta G&=\frac{1}{20k_Frr'}[F(10k_F(r'-r))-(-1)^lF(10k_F(r'+r))] \end{aligned}$$

$F(y)$ is an approximation to $y\int_y^\infty(\cos x/x^2)\,dx$.

[14] K. A. Brueckner and K. S. Masterson, Jr., Phys. Rev. **128**, 2267 (1962).

TABLE V. Values of E_b obtained by solving the K-matrix equations using the usual techniques.[a]

V	E_{ladder}	$E_{\text{Brueckner}}$ $(f=0.1)$	$E_{\text{first order}}$[b]
0	0	0	0
0.0625	2.4415 73584 483	2.4415 91911 4267	2.4415 92505 7001
0.125	4.8278 02569 904	4.8279 41356 8167	4.8279 50061 0416
0.1875	7.1607 22258 662	7.1611 66200 7132	7.1612 07461 6933
0.25	9.4422 65658 171	9.4432 64179 6068	9.4433 87098 0365
0.3125	11.6742 69970 11	11.6761 22607 583	11.6764 06409 188
0.375	13.8584 82583 59	13.8615 27000 580	13.8620 84742 460
0.4375	15.9965 66616 60	16.0011 68776 249	16.0021 49673 596
0.5	18.0901 06045 51	18.0966 52158 572	18.0982 42837 263
0.5625	20.1406 10458 47	20.1495 00394 278	20.1519 25312 047
0.625	22.1495 19464 82	22.1611 61370 376	22.1646 82599 677
0.6875		24.1330 12707 885	24.1379 29234 137
0.75		26.0663 66395 184	26.0730 13052 758
0.8125		27.9624 73014 938	27.9712 19158 194
0.875		29.8225 25610 709	29.8337 73597 385
0.9375		31.6476 63232 903	
1.00		33.4389 74198 271	

[a] All entries are multiplied by 10^8.
[b] Means only first-order terms retained in the single-particle energies.

In solving Eq. (9) we used an 11×11 mesh (10 intervals) and a trapezoidal rule. The same mesh was used in Eq. (10) and the same trapezoidal rule. Equation (11) was integrated with $\Delta k=1/20k_F$ and a Simpson's rule. Equation (13) was integrated with $\Delta m=\frac{1}{10}k_F$ and Simpson's rule.

The single-particle energy tables were interpolated using three points in the Green's functions integration. The energy tables were cut off at $4k_F$. Tests showed this cutoff to be adequate. Contributions to the angular momentum expansion were neglected for $l>2(k_Fc\leqq1)l>3(k_Fc=1.5)$, and $l>4(k_Fc\geqq2)$.

The energy tables were chosen initially to be $E(m)=m^2/2$ for all m; the equations were iterated until the single-particle energy table was self-consistent to 4 decimal places.

For the square-well potential, we may calculate E_b for any number of potential depths, and from the data we may find the series expansion of E_b to any number of terms. Some results are shown in Tables V and VI.

The ladder approximation is obtained by using

$$E(m)=m^2/2 \tag{5.15}$$

instead of Eq. (5.11), and otherwise proceeding in the same way as in the case of the Brueckner theory.

In comparing Table VI with the exact Monte Carlo calculation of these expansions, the only glaring discrepancy is in the value of the coefficient of V^4 for the Brueckner theory. In third order, even the difference between the Brueckner and ladder diagram results obtained from Table VI and the Monte Carlo calculations agree. But this same difference in fourth order obtained from Table II and the Monte Carlo calculations are very different.

This means that the ordinary calculations of the Brueckner theory, as outlined in this section, approximate *each* third-order diagram very well, but not *each* fourth-order diagram. In order to investigate which fourth-order diagram has not been adequately approximated, we have calculated the Brueckner theory, keeping only those terms in the single-particle energies which are *linear* in the potential V, thus omitting from the Brueckner theory the diagrams shown in Fig. 11.

In practice, Eq. (5.12) was replaced by

$$I=\tfrac{2}{3}Vc^3-Vc^3\left[\frac{\sin2kc}{(2kc)^3}-\frac{\cos2kc}{(2kc)^3}\right]. \tag{5.16}$$

The results are shown in Table V. The series expansion of the Brueckner theory, minus the diagrams of Fig. 11, as obtained from Table V and the Monte Carlo calculation agree, as do the differences [(Brueckner theory minus the diagrams of Fig. 11)—(ladder diagrams)] which establishes that one of the diagrams of Fig. 11 is the diagram not adequately approximated in the ordinary calculations of the Brueckner theory.

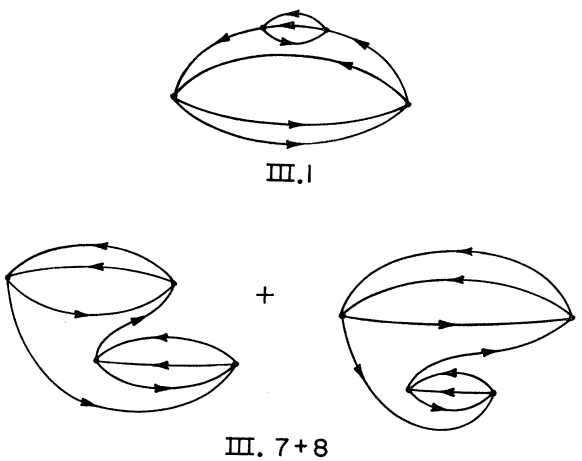

FIG. 11. Diagrams not well approximated by the usual approximate treatment of off-energy shell propagation used in the Brueckner approximation.

TABLE VI. Series expansion for $k_{FC}=1.0$.

E_b (ladder) $=10^{-3}(39.519220V-7.3573749V^2+1.5026353V^3-0.31908594V^4+0.06389859V^5-0.015274886V^6)$

E_b (Brueckner $f=0.1$) $=10^{-3}(39.519220V-7.3573749V^2+1.5820376V^3-0.39131020V^4+0.11601647V^5-0.041403037V^6)$

E_b (Brueckner $f=1.0$) $=10^{-3}(39.519220V-7.3573749V^2+1.5820376V^3-0.36808576V^4+0.09214862V^5-0.024992145V^6)$

E_b (Brueckner $f=3.0$) $=10^{-3}(39.519220V-7.3573749V^2+1.5820376V^3-0.35778685V^4+0.08440648V^5-0.021094986V^6)$

E_b (first order)* $=10^{-3}(39.519220V-7.3573749V^2+1.5820468V^3-0.35285134V^4+0.08047672V^5-0.018638974V^6)$

E_b (ladder from Monte Carlo calculations) $=10^{-3}(39.36174V-7.495V^2+1.538V^3-0.3347V^4)$

E_b (Brueckner from Monte Carlo calculations) $=10^{-3}(39.6174V-7.495V^2+1.619V^3-0.3363V^4)$

* Means only first-order terms retained in the single-particle energies.

The last result could have been anticipated. The introduction of the function F in Eq. (5.5) and the average momentum $\bar{p}$ in Eq. (5.6) are adequate approximations to the effects of the Pauli principle. The coefficient of V is not affected by any of the approximations mentioned at the beginning of this section, and indeed the "Monte Carlo" (actually the coefficient of V is known analytically in the "Monte Carlo" case) result and the results in Table VI for the coefficient V are essentially identical. The coefficient of V^2 is affected by the approximations to the Pauli exclusion effect, but the Monte Carlo results and the results in Table VI are closely the same, so that it has to be expected that the approximations to the Pauli exclusion effects are adequate. The off-energy shell approximations do not enter into third order, or in the fourth-order diagrams other than those shown in Fig. 11. This last statement may be understood as follows. In third order, the only Brueckner diagrams are B3 and F3 [Fig. 2(a), (d)]. The energies of the other particles are not involved in the calculation of the correction to the single-particle energies. In fourth order, the Brueckner diagrams are, in addition to those shown in Fig. 11, I.1, IV.1, IV.2, and IV.3 (Figs. 3 and 8). Again, the energies of the other particles are not involved in the calculation of the corrections to the single-particle energies. But for the diagrams of Fig. 11, the energies of the other particles are involved in calculating a correction to the single-particle energy of one of the particles; that is, the first of Fig. 11 is shown in Fig. 12. In calculating the correction to the energy of Fig. 11, the energy denominator is

$$E(1')+E(1'')+E(2)-E(1''')-E(3)-E(4), \quad (5.17)$$

instead of

$$E(1')+E(1'')-\Delta, \quad (5.18)$$

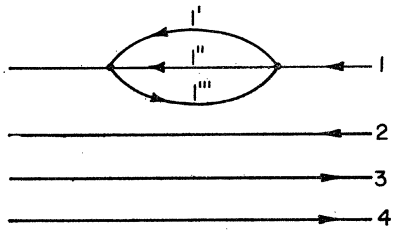

FIG. 12. Middle time segment of diagram III.1.

where Eq. (5.8) specifies

$$\Delta=E(k_F)-f[E(k_F)-E(0)]. \quad (5.19)$$

Equations (5.18) and (5.19) express an approximation to Eq. (5.17), but our results show that the approximation is inadequate.

It is not likely that the difficulty is in the second of the diagrams of Fig. 11, because the actual denominator is (see Fig. 13)

$$E(3')+E(3'')-E(3)-E(3''')$$

because of the two time orders, and, since $|3|<k_F$, Eq. (5.8) is correct subject only to the approximation that the E's are roughly quadratic: that is, there is no off-energy shell effect to approximate.

There is also the point that the total momentum does not disappear from the denominator Eq. (5.18) whereas it does from Eq. (5.17).

We have tried to adjust the value of f in Eq. (5.19) [or Eq. (5.8)] so that the results of the "as-practiced" calculations and the Monte Carlo calculations agree. We have found that no value of $f[0<f<\infty]$ suffices. In the "as-practiced" calculations, the contribution III.1 is negative and greater in magnitude than III.7+8 for example, for $k_{FC}=1.0$.

f	III.1	III.7+8
0.1	-13.63×10^{-5}	9.79×10^{-5}
1.0	-11.31×10^{-5}	9.79×10^{-5}
3.0	-10.28×10^{-5}	9.79×10^{-5}
∞	-9.79×10^{-5}	9.79×10^{-5}

These results were obtained as follows: III.1 was obtained by dropping the inhomogeneous term in Eq. (5.9) and replacing u by j in the right-hand side. Also in Eq. (5.8) the single-particle energies $E(m)$ were

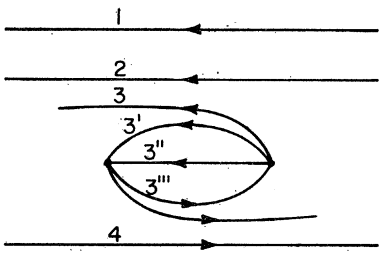

FIG. 13. Middle time segment of diagram III.8.

set equal to $m^2/2$. The modified equations were iterated twice. The first iteration gives B_2, and the second $B_2+\text{III.1}+O(V^6)$.

As f increases without limit, the magnitude of the contribution of III.1 approaches the magnitude of the contribution of III.7+8. This fact may be seen from the table and can be proved analytically. From the Monte Carlo calculations where $k_{FC}=1.0$, we have

III.1	III.7+8
-8.32×10^{-5}	11.55×10^{-5}.

Therefore, although diagrams III.1 and III.7+8 are nominally included in Brueckner theory (the magnitudes of III.1 and III.7+8 are roughly correct when they are considered separately), their sum has the wrong sign because of the treatment of off-energy shell propagation.

Actually $f=\infty$ gives the best possible estimate of their sum (namely zero). We found by direct calculation that the density at which the single-particle energy becomes flat and the self-consistent solution ceases to exist increases as f increases:

$$f=0.1 \quad k_{FC}=2.1$$
$$f=3.0 \quad k_{FC}=2.4.$$

(To obtain these values the approximation $Vu=\lambda\delta(r-c)$ was used. The actual values are somewhat less.) We conclude that it is possible that the self-consistent solution would continue to exist at high density were off-energy shell propagation treated properly. To settle this point, it would be necessary to solve the equations of Appendix A of Brueckner and Gammel[13] in which off-energy propagation is treated exactly.

ACKNOWLEDGMENT

We wish to thank Dr. T. A. Oliphant for kindly checking some of our numerical results on the coefficients in the first three orders, and for his participation in many conversations during the early stages of this work.